Spectral analysis of the lower Eocene Wilkins Peak Member, Green River Formation, Wyoming: Support for Milankovitch cyclicity

M.L. Machlus *, P.E. Olsen, N. Christie-Blick, S.R. Hemming

Department of Earth and Environmental Sciences and Lamont-Doherty Earth Observatory of Columbia University, Palisades, New York 10964, USA

Abstract

This study is the first to employ spectral analysis to examine meter-scale sedimentary cyclicity in the Wilkins Peak Member of the lower Eocene Green River Formation of Wyoming. Generally regarded as the classic example for orbital forcing of lacustrine sediments at eccentricity and precession time scales, this long-standing interpretation was recently contested, with a much shorter duration (≤ 10 ky) inferred for the dominant cyclicity. Earlier work lacked adequate age control or spectral analysis or both. Our analysis is based upon an evaluation in the frequency domain of oil-yield values from four boreholes, accuracy estimation for suggested orbital interpretations, and comparison to independent geochronology. Cored intervals 266–364 m thick represent a span of 1.2–1.7 m.y., with temporal resolution of ~ 3–5 ky (~ 1 m) for oil-yield values. Variations in spectral power with depth within the original records are interpreted to reflect changes in the rate of sediment accumulation. These changes are corrected prior to testing the orbital forcing hypothesis by using two methods: 1) a minimal adjustment (three segments) accounting for the dominant changes of spectral frequency with depth; and 2) correlating the published definitions of precessional cycles in these records to a 21 ky cosine curve. Orbital age models resulting from the two tuning methods are compared to available chronology and the tuned records are tested for the expected spectral peaks from orbitally forced records. We conclude that the dominant cyclicity of the Wilkins Peak Member is orbitally forced. Orbital age models overlap $^{40}Ar/^{39}Ar$ ages and inferred periods include long and short eccentricity, weak obliquity and precession. Eccentricity is resolved in the analyzed records but the expected ~ 95 and ~ 125 ky periods are not resolved, controlling the range of possible tuning periods and the accuracy of orbital age models. Sub-Milankovitch variability exists and can be resolved to a minimum period of ~ 3–5 ky by the analyzed records. However, it cannot be characterized fully with the available chronology or by the previously calculated mean cycle duration.
© 2008 Elsevier B.V. All rights reserved.

Keywords: spectral analysis; Green River Formation; Wilkins Peak Member; Eocene; orbital forcing; tuning

1. Introduction

The lower Eocene Green River Formation has long been regarded as the classic example of orbital forcing in a lacustrine setting (Bradley, 1929). Milankovitch cyclicity has been interpreted in several studies, and in different parts of this formation in Utah, Colorado and Wyoming (e.g., Fischer and Roberts, 1991; Roehler, 1993; Bereskin and Morgan, 2001). In general, these studies describe the cyclicity in the depth domain but lack radiometric age control and spectral analysis. Their common interpretation is that meter-scale sedimentary cycles, reflecting expansion and contraction of Lake Gosiute, were forced by precession of the equinoxes (~ 20 ky) and modulated by short eccentricity (~ 100 ky). However, recent $^{40}Ar/^{39}Ar$ chronology of intercalated ashes within the Wilkins Peak Member of the Green River Formation in Wyoming, combined with cycle counting, has been used to contest this classic view (Pietras et al., 2003; Pietras and Carroll, 2006). Pietras and Carroll (2006) calculated a mean cycle duration of ~ 10 ky for intervals between pairs of dated ashes in their most basinal sections, and concluded that the cycles cannot have been forced by precession.

In this paper we present the first spectral analysis of the Wilkins Peak Member as a test of these competing views.

Evolutionary spectra (frequency and relative power plotted as a function of depth) and total spectra obtained from published numerical core data explicitly permit tests for periodicity or quasi-periodicity, the assignment of statistical significance to spectral peaks, and an evaluation of the full hierarchy of nested cycles that is implied by the orbital forcing hypothesis, including the relative importance of thin cycles compared to thicker cycles. The orbital age models presented here are based on two fundamentally different methods of tuning, one of them includes only three adjustments of the original records. A novel approach is to include an estimate for the possible range of tuning parameters (and hence to estimate the accuracy limits of the approach) for each orbital age model. The resulting floating orbital age models are also tested against available ^{40}Ar/^{39}Ar ages. The possibility of incomplete expression of the cyclicity is discussed.

Testing the orbital origin of Green River Formation cyclicity has implications for timescale calibration, early Eocene climate and mammal evolution. Astronomical calibration of the geological timescale extends back through the Neogene (Lourens et al., 2004a,b), but is limited by the precision of Laskar et al. (2004) orbital solution to ∼40 Ma. If the Milankovitch forcing of climate can be resolved in these lacustrine sediments, high-resolution, long lacustrine records of the Green River Formation may eventually be used to test the orbital solutions at ∼50 Ma. The series of warm events recorded in marine records during the early Eocene was recently related to orbital forcing (Westerhold et al., 2007). Further testing of this hypothesis is possible if a Milankovitch-based timescale is established for the Green River Formation. The lacustrine climate records can also be tied to sites of land mammal fossils at the margin of the lake, improving the time control on mammal evolution and records of magnetic polarity (Clyde et al., 1997; 2001) obtained from these sites.

2. Geological context and prior studies of the cyclicity

The Green River Formation (Hayden, 1869) encompasses Eocene lacustrine strata deposited in several basins in Wyoming, Colorado and Utah (Bradley, 1929; Roehler, 1992a,b; Fig. 1a) during the late stages of the Laramide orogeny (Dickinson et al., 1988; Prothero, 1996; Smith et al., 2008). The

formation is characterized by the inter-stratification of organic-rich, microlaminated micrite and dolomicrite "oil shale", and less organic-rich sediments (Bradley, 1929; Roehler, 1993). Alternations of these deposits constitute "sedimentary cycles", or "cycles," terms that are used here in a purely descriptive sense without implying any particular origin or periodicity in time.

The strata appear to have been deposited in three main lacustrine basins (Fig. 1a): Lake Gosiute (King, 1878; Bradley, 1929) within the Greater Green River Basin (subdivided by contemporaneous and/or younger structures into the Bridger, Washakie, Great Divide and Sand Wash basins; Fig. 1b); Lake Uinta (Bradley, 1929) within the Piceance Creek and Uinta basins; and Fossil Lake (Bradley, 1948; Oriel and Tracey, 1970) in the Fossil Basin. This study focuses on the Wilkins Peak Member of the Green River Formation in Wyoming (Fig. 1c).

The Wilkins Peak Member is the medial evaporite-rich interval of the Green River Formation in Wyoming (Fig. 1b and c). The Tipton Member below and Laney Member above are characterized by abundant oil shale, and are thought to reflect generally fresher lake water and higher lake stands. The Wilkins Peak Member also contains oil shale but as discrete beds within laterally persistent sedimentary cycles that are thought to record changes in the depth and dimensions of Lake Gosiute (e.g., Eugster and Hardie, 1975; Smoot, 1983; Roehler, 1993; Pietras et al., 2003; Pietras and Carroll, 2006). We chose to test the orbital forcing hypothesis on published oil-yield records from the Wilkins Peak Member because ^{40}Ar/^{39}Ar chronology for this interval (Smith et al., 2003, 2006, 2008) allows this test. Ages of ash beds at the top of the Wilkins Peak Member (6th tuff), in the lower part of the member (firehole tuff) and in the middle of the Rife Bed below the studied interval (rife bed tuff) constrain the deposition of the Wilkins Peak Member to ∼1.2 to ∼1.7 m.y. in duration (summary of ages in Smith et al., 2008).

2.1. Numerical proxy for sedimentary cycles

2.1.1. Facies alternations

Wilkins Peak cycles are defined by the following generalized sequence of lithofacies (Eugster and Hardie, 1975; Smoot, 1983; Roehler, 1993; Pietras et al., 2003; Pietras and Carroll,
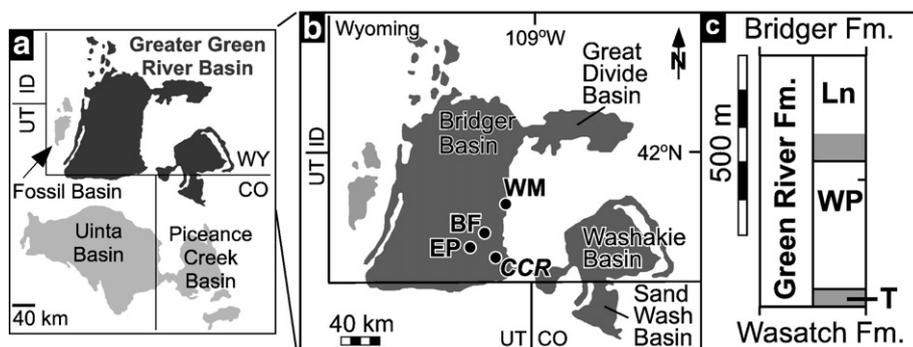

Fig. 1. Location map and general stratigraphy. (a) Extent (shaded) of the Green River Formation (Grande, 1984). (b) Location of cores, and extent (shaded) of the Green River Formation in the Greater Green River Basin (Grande, 1984). Abbreviations of core names: WM, ERDA-LERC White Mountain 1; BF, ERDA-LERC Blacks Fork 1; EP, Union Pacific Rail Road Company El Paso 44-3; and CCR, U.S. DOE/LETC CCR-1 (designated hereafter as WM, BF, EP and CCR, respectively). (c) General stratigraphy for core BF near the center of the Bridger basin (Roehler, 1991a). Shaded intervals are composed mainly of oil shales; Members: T, Tipton; WP, Wilkins Peak; Ln, Laney.

2006): organic-rich micrite ("oil shale"); trona, halite or authigenic evaporite minerals (e.g., shortite) precipitated within bedded micrite; mudcracked dolomicrite; and calcareous sandstone with platy mudstone intraclasts. This sequence is interpreted to represent upward shoaling from deepest to shallowest lake conditions (oil shale to evaporite and mudcracked deposits), followed by renewed deepening (reworking of micrite into intraclasts, and deposition of oil shale at the base of the next cycle). Smoot (1983) noted that vertical transitions within cycles are observed also as lateral arrangements of facies. For example, oil shale in the basin center, bracketed by correlatable ash markers, interfingers with non-laminated mudstone and mudcrack-bearing mudstone near the basin margin.

2.1.2. Oil-yield proxy

Roehler (1993) identified 77 prominent oil shale beds and associated sedimentary cycles in the Wilkins Peak Member (see also Culbertson et al., 1980), and used oil-yield histograms (Roehler, 1991a,b,c) as a numerical proxy for the sedimentary cycles. The oil shale beds are typically 0.3–5 m thick (1 m average), and the cycles in which they are found are 1.6–15.3 m thick (4.2 m average; see Culbertson et al., 1980). In general, oil-yield values correlate with organic matter content (Dyni et al., 1989; Miknis, 1995) and follow the sedimentary cycles that Roehler identified, such that peaks of oil-yield values correspond to oil shale beds.

2.1.3. Lateral persistence

Oil shale beds in the central part of the basin are laterally persistent over distances of several tens of kilometers (Culbertson et al., 1980; Roehler, 1992a and references therein; Culbertson, 1998). Roehler (1991b) used such beds to identify and correlate 77 oil-yield cycles. Pietras et al. (2003) and Pietras and Carroll (2006) mapped additional cycles, counting as many as 126 in core WM (located in Fig. 1b). Several laterally persistent markers support the correlation of prominent oil shale beds: air fall ash layers (Culbertson, 1961; Culbertson et al., 1980; Smoot, 1983; Roehler, 1991b; Pietras and Carroll, 2006), nine mudstone and sandstone units (Culbertson, 1961; Culbertson et al., 1980), and 25 numbered trona beds (Culbertson, 1971).

2.2. Prior assessments of cyclicity in the Wilkins Peak Member

Roehler (1993) suggested that the development of the 77 prominent oil shale beds was orbitally forced by precession of the equinoxes, and that these precessional cycles are grouped into 17 cycles forced by changes in the eccentricity of Earth's orbit (denoted A–Q by Roehler). Fischer and Roberts (1991) suggested a similar interpretation from gamma-ray logs of cores, where gamma-ray values are high in intervals of high organic content, intermediate in marlstone, and lowest in trona. These studies rely on apparent grouping, also known as "bundling" (Hinnov, 2000) of 5 shorter cycles into longer, modulating cycles, as evidence for possible precessional (~20 ky) and eccentricity (~100 ky) forcing.

Pietras et al. (2003) described and counted 42 cycles between dated ashes in Core WM (Fig. 1b) and ruled out precession as the direct forcing of these sedimentary cycles on the basis of a calculated mean period of 10.2±3.6 ky. Pietras and Carroll (2006) extended this reasoning to other dated intervals of the Wilkins Peak Member (126 cycles in core WM) and concluded that random forcing may have been responsible. They did not preclude the existence of precessional cycles, albeit with a longer wavelength than their described cycles.

3. Analyzed records and spectral analysis methods

3.1. Records locations and data sources

Records of oil-yield values studied here are from four cores in a basinal position (Sullivan, 1980; Roehler, 1992a; see Fig. 1b for locations and Fig. 2 for oil-yield records). Most basinal are cores BF and EP (Sullivan, 1980). Cores WM and CCR are slightly more marginal. Importantly, core WM is the most basinal location studied by Pietras and Carroll (2006), thus allowing a direct comparison of the approaches. The data used here were published as oil-yield histograms in Roehler (1991a,b,c). Text files of these data as well as photocopies of unpublished lithological descriptions (cited in Roehler, 1991a,b,c) were obtained from J. R. Dyni (USGS, retired, personal communication, 2000). Text files are available in Appendices B (same format as in Dyni, 1998), C and D.

3.2. Data quality and representation

Oil-yield values were calculated from assay results, obtained from channel samples by the modified Fischer assay method (Stanfield and Frost, 1949) except for low yield samples (<3 gal/ton; see analytical details in Sinks et al., 1983). Oil-yield values are plotted as histograms vs. depth, because each value represents a whole assayed interval corresponding to one continuous channel sample. A few intervals lacking data typically correspond with low oil-yield values, and are thought not to influence the results of the analysis (marked "B0.00" and "NaN" in Appendices B and C respectively).

3.3. Interpolation and scaling

The sampling interval for Fischer assays is variable. So, in order to perform spectral analyses on uniformly spaced data, it was necessary to interpolate the records. The interval chosen for this purpose was 1 ft (0.3048 m), the mean sampling interval and the unit originally used for measuring and describing cores. Consequently, all depth and frequency (depth^{-1}) axes are in feet. Oil-yield values were reported with identical depths for the base and top of consecutive intervals (with the notation of "from", "to" for each oil-yield value for each interval, see Appendix B). In order to maintain this format and to distinguish values at the boundaries between successive intervals, a depth value of 0.001 ft was added to the top of all reported intervals (see Appendix C). For example, if oil yield were reported as 10 gal/ton from 450 ft to 451 ft and 11 gal/ton from 451 ft to 452 ft, the actual values used for spectral analysis are 10 gal/ton for depths of 450.001 ft to 451 ft and 11 gal/ton for depths of 451.001 ft to 452 ft.). Intervals with no data were removed prior to spectral analysis (data in the format used for spectral analysis are available in Appendix D).
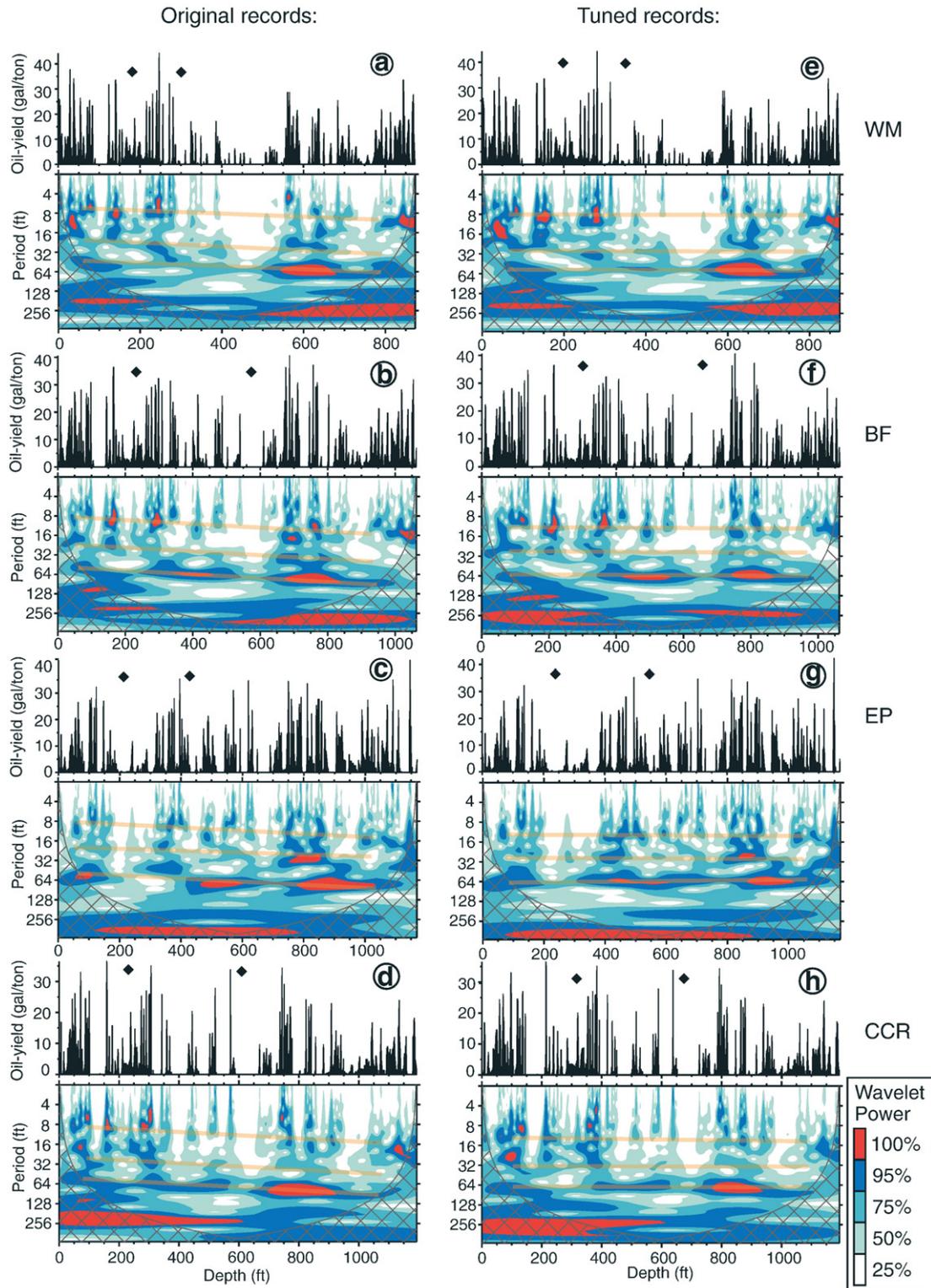
Original records: Tuned records:

Fig. 2. Comparison of evolutionary wavelet spectra for the original, un-tuned record (a–d) with spectra for the record tuned by tuning method 1 (e–h). Oil-yield values from Roehler (1991a,b,c) are shown above each spectrogram, with the locations of tuning points marked by diamonds. The records were interpolated to 0.3048 m (1 ft) intervals prior to the analysis and are shown on feet scale relative to the top of the Wilkins Peak Member. Curved black lines and hachured area outline the cone of influence on the spectrograms, where edge effects become important. Tuning is preformed by changing the lengths of two segments, located above and below the tuning points, relative to the length of the middle segment. The adjustment amount is such that the corresponding three maxima for power ridges along the lowermost yellow line are aligned. Parallel lines on each spectrogram delineate approximately parallel ridges of power with increasing period as a function of depth within original records that may indicate a change in sedimentation rate (note that the period scale is logarithmic). Periods of same ridges of spectral power in tuned records are invariant with depth.

3.4. Spectral analysis methods and software

Evolutionary wavelet spectra were obtained according to the method described in Torrence and Compo (1998) using a modified version of their Matlab© script, their interactive web-based program (http://paos.colorado.edu/research/wavelets/) and a Morlet wavelet with a wave number of 6.

Multi-Taper Method (MTM) spectra were calculated by the SSA-MTM Toolkit (Ghil et al., 2002) using 3 tapers and resolution of 2. Background estimate and hence confidence levels are based on a robust red noise estimation, as described in Mann and Lees (1996).

4. Methodology for testing the orbital forcing hypothesis

The test is composed of the following five steps: 1) spectral analysis of the original records (Section 4.1); 2) tuning the records and spectral analysis of the tuned records (Sections 4.2–4.3); 3) calculation of orbital age models (Sections 4.2–4.3); 4) comparison of significant periods within the tuned records to the expected periods from orbitally forced records (Sections 5–6); and 5) comparison between orbital age models and independent radiometric ages (Sections 5–6).

The first 3 steps are part of an iterative process where evaluation of results from the first and second steps determine the methods used in the second and third steps respectively; therefore steps one through three are grouped here as part of the methodology section. Orbital tuning is central to this test. Therefore we outline below the rationale, methods and potential caveats that are relevant for the tuning methods we use. A general explanation of the motivation for using spectral analysis and summary of expected orbital periods is provided in Appendix A.

4.1. The need for tuning: correcting for changes in sediment accumulation rates

Tests for orbital forcing can fail even for an orbitally forced record if sediment accumulated at varying rates and if no correction is made for those variations. Among undesirable consequences of non-uniform sediment accumulation are the broadening of spectral peaks and the appearance of periods unrelated to orbital forcing (see Fig. 4 of Hinnov, 2000). Our first step in evaluating the cyclicity is therefore to determine if there is any need for modifying the original depth scale.

Spectrograms of the four records (Fig. 2a–d) show peaks of spectral power that, for a given depth range, have the expected ratio of periods for orbital forcing. However, they yield increasing periods with depth, in contrast to the expected constant periods from an orbitally forced record with constant sedimentation rate. We therefore proceed with orbital tuning.

4.2. Tuning: two general approaches

Tuning the record involves modifying the original depth scale according to *a priori* assumptions in order to correct for apparent changes in sediment accumulation rate. We use two tuning methods, similar to two general approaches: tuning in the frequency domain (e.g., Preto and Hinnov, 2003) and tuning with specific cycle period(s) (e.g., Hilgen et al., 1995; Pälike et al., 2006a; Westerhold et al., 2007). Fewer adjustments are needed in the frequency domain. We minimize circular reasoning that is inherent to orbital tuning, by using both a small number of assumptions and by assigning error estimates to the chosen tuning parameters and orbital age models.

4.3. Tuning methods and orbital age models

4.3.1. Tuning method 1

The tuned record is constructed using only three adjustments according to five chosen parameters: Two tuning points define three parts of the record (diamonds in Fig. 2) centered between power ridges that exhibit a maximum change in wavelength. The lengths of the two outer parts of the record are adjusted, relative to the length of the central segment and the result is scaled to the original length. The result is a better alignment of spectral peaks versus depth for the tuned records, compared to the original spectrograms, thereby providing adequate records for the next step of calculating orbital age models and testing the cyclicity (Fig. 2). The motivation for choosing these particular adjustments is to minimize *a priori* assumptions and subjective choices and to simplify error estimation for each chosen value. The tuning process and reasoning for each choice are detailed below.

The underlying assumption of the tuning is that spectral peaks with wavelengths of ∼40 to ∼80 ft, belong to a single periodicity (see spectral ridges around bottom line in Fig. 2a–d). This specific range of wavelengths is selected out of three possible bands of spectral peaks for which wavelength appears to increase with depth (yellow lines in Fig. 2a–d around 64 ft, 32 ft, 16–8 ft; note that the period axis is a logarithmic scale). Spectral peaks are less well defined at shorter wavelengths than at longer ones. However, the longest wavelength (∼256 ft) corresponds with underestimated power due to the addition of zeros to the original data ("zero-padding"), a step that is needed for spectrum estimation of a given (long) interval (the "edge effect area" marked by hachures in Fig. 2). The optimal choice for the tuning band is therefore within periods of ∼40 to ∼80 ft.

The relevant parameters for tuning are chosen according to prominent power ridges, each characterized by a period that increases with depth within the tuning band (between the periods of ∼40 to ∼80 ft, in Fig. 2a–d). Tuning points that divide the record into three segments are positioned at power minima, where the most pronounced changes in wavelength occur (pronounced in cores BF, EP, CCR and less clear in core WM; Fig. 2a–d). The power ridges are forced into a single periodicity by scaling the length of the upper and lower segments relative to the middle segment according to ratios of periods, taken at the power maximum within each segment.

For example, within core BF the tuning is as follows: between the top of the Wilkins Peak Member (0 ft) and 229.9 ft, the depth differences were multiplied by 59.7/48.5 or 1.23 to raise the average apparent period for the respective spectral ridge from 49 to 60 ft, the middle power ridge at a period of ∼60 ft was not adjusted, and for depths between 572.7 and

1063.1 ft, the depth intervals were multiplied by 59.7/76.1 or 0.78 to decrease the average apparent period from 76 to 60 ft. The resulting total core "length" is shorter than the original total, and the converted record is scaled back to the original length (324 m, 1063.1 ft for core BF). This last step scales the period of the aligned power to 64 ft. A similar procedure is applied to the other records, and the tuned records (Fig. 2e–h) thus contain aligned spectral peaks around the tuning period of about 64 ft (frequency of 0.0156 ft^{-1}; see yellow lines in Fig. 2e–h).

The statistical significance of the power ridges selected for alignment cannot be estimated well, owing to the difficulty in characterizing the background noise. Using the extreme assumption of white noise background (i.e., un-correlated noise), all chosen power peaks are significant above the 5% significance level. Using the conventional assumption of red noise the power ridges within the following segments are significant at the 5% level: the upper and lower segments of cores EP and CCR, the middle and lower segments at core BF, and the lower segment at core WM (see Appendix E). However, the assumption of red noise leads to an overestimate of the background for these records, owing to the intervals of zero oil-yield values (e.g., 300–500 ft in WM and 300–700 ft in CCR).

Calculated orbital age models are therefore used as an alternative procedure for evaluating statistical significance. The choice of specific spectral peaks for alignment translates into the two main errors associated with the orbital age models. Imperfect alignment choices, such as the selection of one ridge in preference to a neighboring one, lead to smearing of spectral peaks and hence to the two large errors described below (Section 4.3.2). Substituting a range of values for the selected tuning parameters leads to a much smaller error (Section 4.3.2).

The orbital age models for all tuned records are calculated by equating the tuning period (∼64 ft) with the eccentricity period (chosen as 105 ky, although note that a range of 95 to 125 ky is discussed in Section 4.3.2 below). The spectrograms for the tuned records reveal several parallel bands of spectral power with approximately constant period (yellow lines marked on wavelet spectra in Fig. 2e–h), in addition to the power concentrated along the tuning period (bottom line on wavelet spectra in Fig. 2e–h). The multi-taper power spectra produced with this approach (Fig. 3) contain significant peaks with ratios that are similar to the expected ratios from orbitally forced records. If these ratios reflect orbital forcing, the tuning period for each record may be identified with eccentricity and allow the construction of orbital age models. The tuned records (in depth units) are thus converted into orbital age models (in time units; dashed lines in Fig. 4) by assuming that the period of the significant peak associated with the tuning period (marked by a star in Fig. 3) corresponds to eccentricity.

4.3.2. Error estimation for tuning method 1

The largest errors associated with tuning method 1 originate from two related tuning parameters. First, the period chosen for eccentricity can range between ∼95 and ∼130 ky (see Appendix for a summary of periods) and defines accordingly a range of orbital age models for each tuned record (three dashed lines in Fig. 4). Periods of about 95 and 125 ky appear in
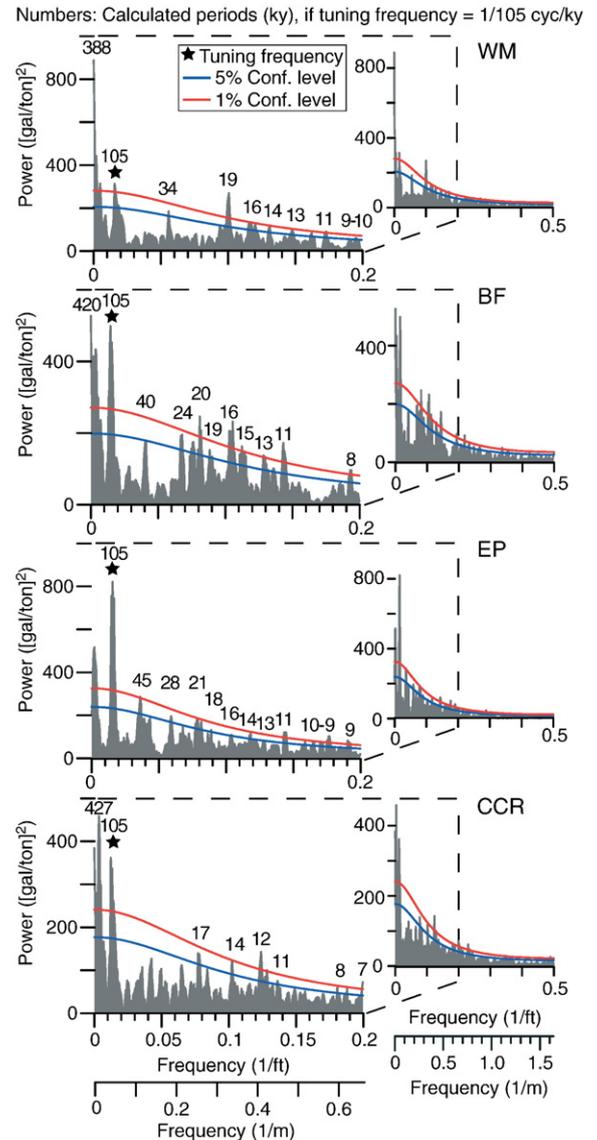

Fig. 3. Multi-Taper Method (MTM) spectra of the tuned records using tuning method 1. Numbers denote the calculated "periods" resulting from assumed eccentricity period of 105 ky for the tuning period. Expected periods from orbitally forced records based on the present are as follows: for precession, mainly 19 ky, 22 ky and 24 ky; 41 ky for obliquity; mainly 95 and 125 ky for short eccentricity (95, 99, 124 and 131 ky) that are often combined into ∼100 ky; 404 ky for long eccentricity (see summary in Hinnov, 2000; 2004; see also Appendix A).

orbitally forced records (e.g., Triassic: Olsen and Kent, 1999; Oligocene: Pälike et al., 2006b). Two double spectral peaks around 95 and 125 ky also dominate the eccentricity parameter for the last 50 m.y. according to Laskar et al. (2004) solution for this parameter (calculated by AnalySeries (Paillard et al., 1996) and also available at http://www.imcce.fr/Equipes/ASD/insola/earth/earth.html). These dominant periods are not resolved in the oil-yield records, placing the apparent eccentricity period anywhere between these periods. We therefore chose the two dominant periods (95, 125 ky) and an intermediate value (105 ky) to represent the actual resolution of the studied records and hence the accuracy of the orbital age models.
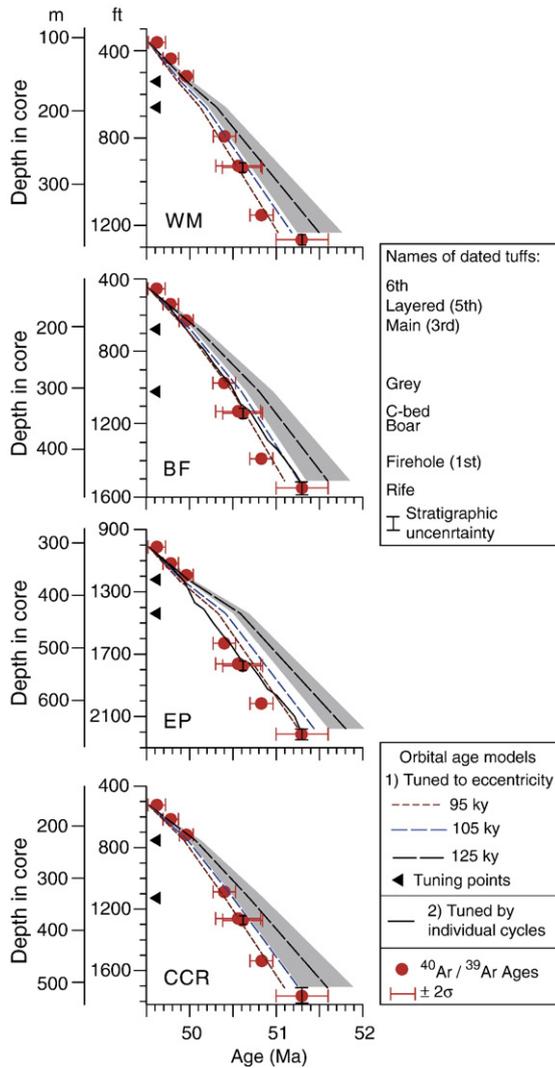
Fig. 4. Orbital age models for cores WM, BF, EP and CCR compared to $^{40}Ar/^{39}Ar$ ages of Smith et al. (2003, 2006, 2008). Error bars for $^{40}Ar/^{39}Ar$ ages are the reported 2σ while vertical bars are stratigraphic uncertainties (see Appendix A for stratigraphic details). Three orbital age models are shown (in dashed lines), for three different values chosen for the tuning period (assumed to be the eccentricity cycle): 95, 105 and 125 ky. Shaded area around the 125 ky age model indicates the accuracy estimate for the period value in depth units before it was converted to time units. This error estimate and shaded area applies for the 95 and 105 age models as well (not shown for clarity). Solid line curves correspond with orbital age model based on cycles A–Q of Roehler (1993) for cores EP and BF. Error estimates for the solid line curves are similar in size to the shaded area around the 125 ky age model (not shown for clarity).

An additional large error is associated with the tuning period (~ 64 ft) that is converted to eccentricity period in order to construct the orbital age model. The resolution of the apparent eccentricity peak for each record (i.e., the width of the significant spectral peak) determines the error associated with the corresponding period. The resolution is calculated as the half-width of the spectral peak at its half-maximum value (Muller and MacDonald, 2000) and translates to a maximum error of about ± 0.2 m.y. per calculated age model. Here we show the range of age models associated with the 125 ky orbital age model for each core and note that this range is applicable to

the 95 ky and 105 ky age models as well, although it is not marked for clarity (see gray zone around the 125 ky model in Fig. 4).

Two additional tuning parameters are adjustable, but the resulting range of orbital age models is small (Fig. 5). These parameters are the location of the tuning points in depth and in period (i.e., x and y axes of the evolutionary spectra of Fig. 2a–d, respectively), and they are constrained by the requirement of constant power with depth in the tuned record. This constraint corresponds with a range of ± 20 ft for the depth range of the tuning points in core BF and a range of 10 to 15% around the chosen period values. The most extreme orbital age models associated with changing each parameter are so small (Fig. 5), that we do not consider these age models any further.

Finally, a limitation that is not fully quantified exists at the edges of the wavelet spectra, where there is not enough information to estimate the full spectrum (often referred to as "edge effect," see hachured area on all wavelet spectra of Fig. 2). Accordingly, each orbital age model is extrapolated, and therefore uncertain in approximately the outer 10% of both ends of the record.

4.3.3. Tuning method 2

The second method relies directly on the cycles that were defined by Roehler (1993) and is implemented for the most basinal cores (BF, EP; see solid curves in Fig. 4 for the respective age models). The Fischer assay record is tied to a target curve, chosen to be a cosine wave with 21 ky period. Seventeen tie points are assigned at the maxima of bundled short cycles (Fig. 6), coinciding with the 17 cycles A–Q of Roehler (1993). Each maximum is tied to each fifth peak of the cosine curve, preserving Roehler's assumption of 5:1 bundling of the meter-scale cycles. We chose not to use an insolation target curve, because the solution for past values of orbital parameters is less precise beyond ~ 40 m.y. ago (Laskar et al.,
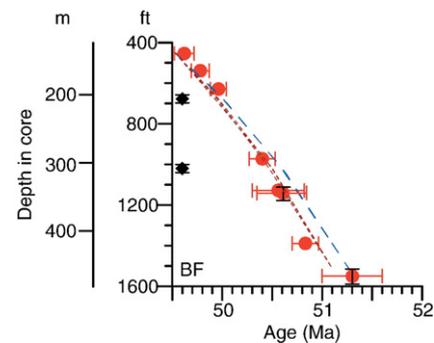

Fig. 5. Small errors associated with tuning parameters of the first tuning method (shown for BF record only). Two groups of orbital age models are shown, resulting from two variations in tuning parameters: 1) Age models in short dashed lines correspond to ± 20 ft (~ 6 m) change in the depth of the two tuning points (age models calculated by the 95 ky value of eccentricity). Diamonds mark the tuning points, with bars denoting depth range of ± 20 ft (~ 6 m). 2) Age models in long dashed lines represent variations in the alignment period, used to align power ridges of the evolutionary spectrum for core BF record (bottom slanted line on wavelet spectrum in Fig. 2b). These age models are calculated by the 105 ky value of eccentricity. $^{40}Ar/^{39}Ar$ ages are shown for comparison (see Fig. 4 for details).
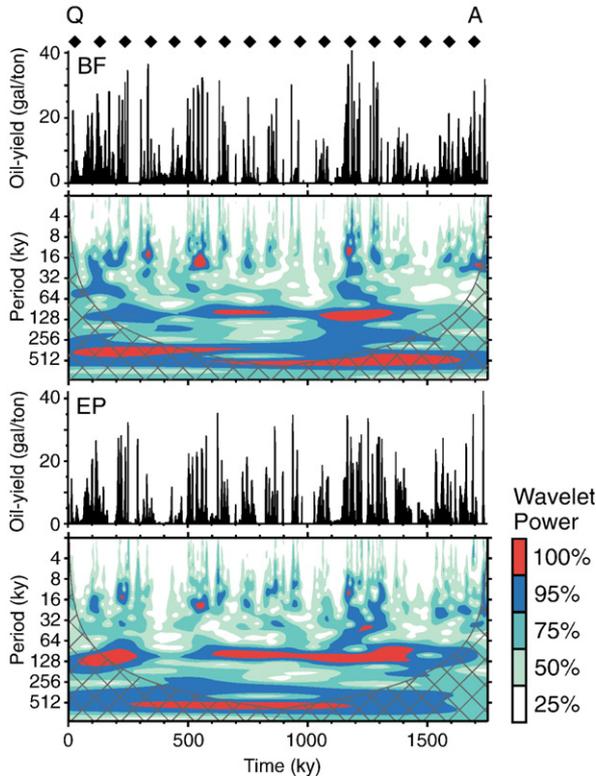
Fig. 6. Evolutionary wavelet spectra and oil-yield values for the second tuning method. Wavelet spectrograms and tuned oil-yield records are for cores BF and EP, tuned to a 21 ky cosine curve according to Roehler (1993) A–Q cycles. Tuning points for these cycles are marked by diamonds. For method detail and original records see Fig. 2.

2004; see also Pälike et al., 2004; Westerhold et al., 2007). Furthermore, generating such a target curve requires assumptions about the exact forcing mechanisms, which we are not confident to infer at this stage.

Both precession- and eccentricity-related periods are associated with this tuning. The usefulness of this method in testing the hypothesis with the spectra alone is therefore limited to other apparent spectral peaks (obliquity, long eccentricity; see spectra in Fig. 7). The age models calculated by this tuning are consistent with both the 95 and 105 age models of the first tuning approach (compare solid curves with the short- and middle-dashed curves in Fig. 4 for BF and EP records).

4.3.4. Error estimation for tuning method 2

Errors associated with tuning method 2 are related to the choice of the tuning target curve and to uncertainties in cycle selection. The target curve can relate to three main precession peaks, with periods of approximately 19, 22, 23 ky during the early Eocene [calculated using AnalySeries (Paillard et al., 1996) and Laskar et al. (2004) values for precession parameters between 50 and 55 Ma]. We chose a middle value of 21 ky. Periods of 19 or 23 ky would result in a change of about 10% in the tuning period. This range in possible tuning periods would therefore correspond with a 10%, or ±0.16 m.y. uncertainty in a 1.6 m.y. interval. Misidentification of cycles adds to this error but is beyond the scope of this study, considering the limitation of this tuning method for testing the orbital forcing hypothesis.

4.3.5. Choosing an anchor point for the orbital age models

The orbital age models for both tuning methods (Fig. 4) are floating, i.e. they represent relative ages within the record. In order to enable the comparison to $^{40}Ar/^{39}Ar$ ages of Smith et al. (2003, 2006, 2008), the orbital models are pinned to the age of the sixth tuff, which is located at the top of the Wilkins Peak Member (see youngest age in Fig. 4). The floating age models could be pinned to the oldest edge of the record, but that approach involves three difficulties in this case: 1) The oldest age within the Wilkins Peak (age of the Firehole tuff, second oldest age in Fig. 4) seems to deviate from the main trend formed by the other ages. 2) The stratigraphic location of the oldest age is uncertain (age of the Rife tuff, located within the Rife Bed that underlies the Wilkins Peak Member). 3) The reported errors for the oldest age are relatively large compared to the younger ages.

5. Results

Significant peaks (at the 5% level) in each tuned record of tuning method 1 have the following frequency ratios relative to the value of 105 chosen for the tuning frequency (Fig. 3): 830:388:105:34:19–9 (WM); 873:420:105:40:24–19:16–15:13–11:8 (BF); 960:105:45:28–18:16–13:11:10–9 (EP); and 872:427:105:17:14:12–11:8–7 (CCR). Additional peaks of 34:22–17 in core CCR are significant only at the 10% level. The actual tuning is independent of any exact value for eccentricity period; therefore the resulting "frequency" axis is in $depth^{-1}$ units.

Significant peaks (at the 5% level; Fig. 7) for each tuned record of tuning method 2 are at periods of 877, 410, 98, 21–15,
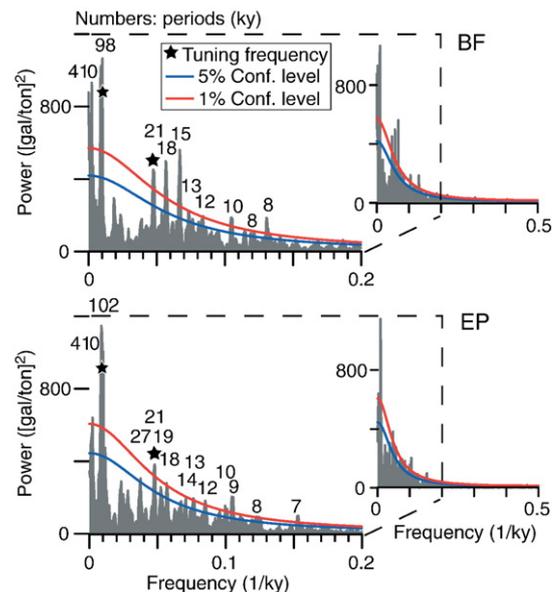

Fig. 7. Multi-Taper Method (MTM) spectra of the two tuned records using tuning method 2. Records from cores BF and EP were tuned by cycle maxima A–Q of Roehler (1993) to a cosine with a 21 ky period, and taking only every 5th cycle (preserving the 5:1 ratio identified by Roehler). Spectral analysis methods are the same as described in Fig. 3, except that the frequency axis here is in $time^{-1}$ units.

13–8 ky/cycle for core BF, and 410, 102, 27, 21–18, 14–7 ky/cycle for core EP.

Orbital age models (Fig. 4) are compared to $^{40}Ar/^{39}Ar$ ages of Smith et al. (2003, 2006, 2008) by correlating dated tuffs to the relevant cores (see details in Appendix A). Stratigraphic uncertainties exist for the boar and rife tuffs (vertical error bars in Fig. 4).

6. Discussion

Our results support the orbital origin for the dominant cyclicity, based on the match between orbital age models and $^{40}Ar/^{39}Ar$ ages, as well as derived ratios of significant peaks that are expected from orbital theory and the structure of the evolutionary spectra. Although sub-Milankovitch variability can be resolved with the oil-yield records, the evaluation of its relative variability as well as the exact frequency of these "cycles" is limited by insufficient resolution of the available chronology. Small differences in the results between the four analyzed records are attributed to erosion of cycles, as Pietras et al. (2003) suggested. However, the number of completely "missing" cycles cannot be large and cannot lead to a rejection of the orbital hypothesis, because of the excellent match among the records and between the orbital age models and $^{40}Ar/^{39}Ar$ ages.

6.1. Suitability and limits of oil-yield values for testing the orbital hypothesis

The completeness of the record and the practicality of testing possible orbital forcing were questioned by Pietras et al. (2003) and Pietras and Carroll (2006), based on the study of mostly marginal locations of the upper Wilkins Peak Member in the northeastern Green River Basin (see also Eugster and Hardie, 1975). Indeed, exposure surfaces are common within the hypothesized precessional cycles and the number of cycles decreases towards marginal locations (Pietras et al., 2003; Pietras and Carroll, 2006). These findings support our interpretation of differences between analyzed records as possible local incompleteness of the record.

Oil-yield values are sufficient for testing the orbital forcing hypothesis but are a limited proxy for characterizing sub-Milankovitch variability at millennial or shorter timescales (~3–5 ky). Many sedimentary cycles are too thin to be captured by the oil-yield values (~0.1–0.2 m; Pietras et al., 2003), most of which were obtained from continuous "channel" samples about 1 ft (0.305 m) long. However, hypothesized precessional cycles are typically ~4 m thick, more than ten times the sampling resolution of oil yields (Roehler, 1993), and most prominent oil shale beds were sampled discretely. For both reasons, oil yield is thought to capture the dominant cyclicity. The thinnest cycle that can be resolved by a minimum of three points is about 3 ft (~1 m) thick, corresponding to approximately 4 to 5 ky. Therefore the reported ~10 ky cyclicity (Pietras et al., 2003; Pietras and Carroll, 2006) can be resolved by the oil-yield proxy, but a full evaluation of the sub-Milankovitch band is not possible.

6.2. Results supporting orbital origin

The arguments in support of the orbital hypothesis are grouped into three lines of evidence that are common to all records: 1) A link between the different apparent cycles is suggested by bands of spectral power that are parallel in evolutionary spectra of the original and tuned records (Figs. 2,6). Within the tuned records, power bands that are independent of the tuning have more constant period with depth, as expected from orbitally forced cycles. 2) Total spectra obtained by Multi-Taper Method (MTM spectra) for both tuning methods generally show significant peaks with common ratios of about 900:400:100:40–30:20, with a few exceptions that are discussed below (Figs. 3,7). These ratios can therefore correspond to long and short eccentricity (100, 400 ky), obliquity (40 ky), precession (20 ky) and possibly the modulator of obliquity (1 my). 3) The match between the radio-isotopic ages and the orbital age models is apparent in Fig. 4. The 95 and 105 ky age models and the age models that are based directly on the cycles overlap the $^{40}Ar/^{39}Ar$ ages, when the error associated with the tuning period is included (grey shaded area in Fig. 4). The 125 ky age models overlap with most of the $^{40}Ar/^{39}Ar$ ages for all records except for the record from EP core.

6.3. Evidence for incomplete record of the cyclicity

Possible partial erosion of cycles is consistent with the observation that cycles are less well developed in cores WM and CCR, even though the discrete oil shale beds associated with the meter-scale sedimentary cycles are identified in all analyzed cores (Culbertson et al., 1980; Roehler, 1991b). Less developed cycles result in less pronounced power ridges in the evolutionary spectra for these cores (e.g., central part of WM and CCR records in Fig. 2) and lower significance levels in the total spectra (e.g., frequencies corresponding to ~34 ky, 17–22 ky for core CCR in Fig. 3). In addition, the tuned record of core WM shows the least improvement over the un-tuned record in comparison to the more basinal cores (Fig. 2), suggesting that the recorded cyclicity may be incomplete or eroded. The slightly shorter period for the interpreted obliquity cycle in cores WM and CCR is attributed to partial erosion of cycles. An apparent obliquity cycle appears as significant peak in the tuned BF and EP cores (by method 1; Fig. 3), at a significance level of slightly less than 90% in core EP tuned by Roehler's cycles (method 2; Fig. 7) and as a weak power ridge in the evolutionary spectrum of core BF (method 2; Fig. 6).

Additional evidence for incompleteness is the shorter calculated length for tuned marginal records of the first tuning method. The shortest estimate is for core WM, slightly longer for cores CCR and BF, and longest for core EP. This change in length is consistent with apparent shorter period for eccentricity cycles in the marginal cores, since the orbital age models and the calculated length are based on the apparent eccentricity period.

6.4. Sub-Milankovitch variability

We agree with Pietras and Carroll (2006) that sub-Milankovitch variability exists throughout the Wilkins Peak Member, but differ in concluding that the available ages do not

allow precise estimation of periodicities and relative variance within the sub-Milankovitch band (regardless of proxy used). These conclusions are due solely to different analytical methods.

The method of simple cycle counting and averaging (Pietras et al., 2003; Pietras and Carroll, 2006) cannot fully describe the variability in the frequency domain (see Appendix A for a detailed comparison of analytical methods). If the assemblage of recognizable sedimentary cycles reflects more than one forcing process, then the mean period is expected to depart from that associated with any individual phenomenon. Therefore a value of ∼ 10 ky mean period is not comparable to the results presented here and may not represent any physical process.

Spectral analysis shows several sub-Milankovitch spectral peaks, but does not allow precise characterization of the sub-Milankovitch variability for two main reasons. First, the sub-Milankovitch periods reflect the errors associated with the chosen eccentricity period. For example, if the 125 ky orbital age model is "correct," then an apparent 15 ky period calculated relative to 105 ky orbital age model will change to about 18 ky (see significant peaks at between 11 and 17 ky in the tuned records, Fig. 3). Second, the objective of minimal tuning and using minimal number of tuning points (i.e., assumptions) leads to too few and only general corrections for changes in sediment accumulation rates. Therefore any short-term changes in sediment accumulation rates that are not corrected by tuning will bias the apparent periods in the total spectra. The minimal tuning method employed here (tuning method 1) is based on the apparent eccentricity period, and is therefore a less effective correction for much shorter periods, such as precession or higher-frequency variability. Thus, determining the sub-Milankovitch variability will require more precise ages spread more densely within the Wilkins Peak Member.

7. Conclusions

Spectral analyses and tuning performed on four oil-yield records, combined with independent $^{40}Ar/^{39}Ar$ dating (Smith et al., 2003, 2006, 2008), demonstrate that sedimentary cycles in the Wilkins Peak Member are most parsimoniously interpreted as orbital in origin. We report for the first time the existence of the 404 ky eccentricity cycle and possible weak obliquity and the long modulator of obliquity, in addition to confirming the suggestions of previous studies for the existence of short eccentricity and precession.

The range of possible tuning periods at ca. 100 ky is the parameter that most strongly controls the errors associated with the orbital age models. More precise ages are required, especially in the lower part of the Wilkins Peak Member, in order to distinguish between orbital age models based on different periods for eccentricity.

Slight differences among the analyzed records are interpreted to be the result of partial erosion of cycles. This interpretation, however, does not preclude orbital forcing, as demonstrated by the close match between the published chronology and our floating orbital age models.

Sub-Milankovitch variability appears to exist, but cannot be characterized fully by the current chronology. The average ∼ 10 ky cyclicity calculated by previous studies (Pietras et al., 2003; Pietras and Carroll, 2006) may not represent any single forcing process and therefore should be interpreted only as an indicator for the existence of sub-Milankovitch variability.

Further testing of longer records is required to validate the persistence of obliquity and the possible ∼ 1 m.y. modulator of obliquity. Such testing is feasible for the Green River Formation in other basins, such as the relatively deep lacustrine environments of the Piceance Creek Basin, also hypothesized to be orbitally forced (e.g., Bradley, 1929; Fischer, 1986; Cole, 1998).

Acknowledgements

Appendix A. Supplementary data

Supplementary data associated with this article can be found, in the online version, at doi:10.1016/j.epsl.2007.12.024.

References

Bereskin, S.R., Morgan, C.D., 2001. Fluvial-lacustrine oil reservoirs in the middle member of the Eocene Green River Formation, south-central Uinta Basin, Utah. AAPG annual meeting. AAPG Bull., 85. Supplement.

Bradley, W.H., 1929. The varves and climate of the Green River epoch. U. S. Geol. Surv. Prof. Pap. 158, 87–110.

Bradley, W.H., 1948. Limnology and the Eocene lakes of the Rocky Mountain region. Geol. Soc. Amer. Bull. 59, 635–648.

Clyde, W.C., Zonneveld, J.P., Stamatakos, J., Gunnell, G.F., Bartels, W.S., 1997. Magnetostratigraphy across the Wasatchian/Bridgerian NALMA boundary (early to middle Eocene) in the western Green River basin, Wyoming. J. Geol. 105, 657–669.

Clyde, W.C., Sheldon, N.D., Koch, P.L., Gunnell, G.F., Bartels, W.S., 2001. Linking the Wasatchian/Bridgerian boundary to the Cenozoic global climate optimum; new magnetostratigraphic and isotopic results from South Pass, Wyoming. Palaeogeogr. Palaeoclimatol. Palaeoecol. 167, 175–199.

Cole, R.D., 1998. Possible Milankovitch cycles in the lower Parachute Creek Member of Green River Formation (Eocene), north-central Piceance Creek basin, Colorado; an analysis. In: Pitman, J.K., Carroll, A.R. (Eds.), Modern & Ancient Lake Systems; New Problems and Perspectives. Utah Geological Association, Salt Lake City, United States, pp. 233–259.

Culbertson, W.C., 1961. Stratigraphy of the Wilkins Peak member of the Green River Formation, Firehole Basin Quadrangle, Wyoming, Article 348. U. S. Geol. Surv. Prof. Pap. 424-D, 170–173.

Culbertson, W.C., 1971. Stratigraphy of the trona deposits in the Green River Formation, southwest Wyoming. Contrib. Geol. 10, 15–23.

Culbertson, W.C., Smith, J.W., Trudell, L.G., 1980. Oil Shale Resources and Geology of the Green River Formation in the Green River Basin, Wyoming. Laramie Energy Technology Center LETC/RI-80/6. 102 pp.

Culbertson, W.C., 1998. Road log for the geology field trip of June 13, 1997; geology and outcrops of the trona bearing rocks of the Green River Formation. In: Dyni, J.R., Jones, R.W. (Eds.), Proceedings of the First International Soda Ash Conference; Volume II. Public Information Circular — Geological Survey of Wyoming. Geological Survey of Wyoming, Laramie, Wyoming, United States, pp. 205–211.

Dickinson, W.R., Klute, M.A., Hayes, M.J., Janecke, S.U., Lundin, E.R., McKittrick, M.A., Olivares, M.D., 1988. Paleogeographic and paleotectonic setting of Laramide sedimentary basins in the central Rocky Mountain region. Geol. Soc. Amer. Bull. 100, 1023–1039.

Dyni, J.R., 1998, Fischer assays of oil-shale drill cores and rotary cuttings from the Piceance Creek basin, Colorado, version 1. US Geol. Surv. Open-File Report OF 98-0483, 1 disc.

Dyni, J.R., Anders, D.E., Rex, R.C., 1989. Comparison of hydroretorting, Fischer assay, and Rock-Eval analyses of some world oil shales. Proceedings of the 1989 Eastern Oil Shale Symposium, November 15–17, 1989. University of Kentucky Institute for Mining and Minerals Research, Lexington, Kentucky, pp. 270–286.

Eugster, H.P., Hardie, L.A., 1975. Sedimentation in an ancient playa-lake complex; the Wilkins Peak Member of the Green River Formation of Wyoming. Geol. Soc. Amer. Bull. 86, 319–334.

Fischer, A.G., 1986. Climatic rhythms recorded in strata. Annu. Rev. Earth Planet. Sci. 14, 351–376.

Fischer, A.G., Roberts, L.T., 1991. Cyclicity in the Green River Formation (lacustrine Eocene) of Wyoming. J. Sediment. Petrol. 61, 1146–1154.

Ghil, M., Allen, M.R., Dettinger, M.D., Ide, K., Kondrashov, D., Mann, M.E., Robertson, A.W., Saunders, A., Tian, Y., Varadi, F., Yiou, P., 2002. Advanced spectral methods for climatic time series. Rev. Geophys. 40.

Grande, L., 1984. Paleontology of the Green River Formation, with a review of the fish fauna. Bull. Geol. Surv. Wyo 63, 333pp.

Hayden, F.V., 1869. Preliminary Field Report of the United States Geological Survey of Colorado and New Mexico. Government Printing Office, Washington, p. 155 pp.

Hilgen, F.J., Krijgsman, W., Langereis, C.G., Lourens, L.J., Santarelli, A., Zachariasse, W.J., 1995. Extending the astronomical (polarity) time scale into the Miocene. Earth Planet. Sci. Lett. 136, 495–510.

Hinnov, L.A., 2000. New perspectives on orbitally forced stratigraphy. Annu. Rev. Earth Planet. Sci. 28, 419–475.

Hinnov, L.A., 2004. Earth's orbital parameters and cycle stratigraphy. In: Gradstein, F.M., Ogg, J.G., Smith, A.G. (Eds.), A Geologic Time Scale 2004. Cambridge University Press, Cambridge, UK, pp. 55–62.

King, C., 1878. Systematic Geology. United States Geological Exploration of the Fortieth Parallel. Government Printing Office, Washington. 803 pp.

Laskar, J., Robutel, P., Joutel, F., Gastineau, M., Correia, A.C.M., Levrard, B., 2004. A long-term numerical solution for the insolation quantities of the Earth. Astron. Astrophys. 428, 261–285.

Lourens, L., Hilgen, F.J., Shackleton, N.J., Laskar, J., Wilson, D., 2004a. The Neogene period. In: Gradstein, F.M., Ogg, J.G., Smith, A.G. (Eds.), A Geologic Time Scale 2004. Cambridge University Press, Cambridge, UK, pp. 409–440.

Lourens, L., Hilgen, F.J., Shackleton, N.J., Laskar, J., Wilson, D., 2004b. Orbital turning calibrations and conversions for the Neogene period. In: Gradstein, F.M., Ogg, J.G., Smith, A.G. (Eds.), A Geologic Time Scale 2004. Cambridge University Press, Cambridge, UK, pp. 469–484.

Mann, M.E., Lees, J.M., 1996. Robust estimation of background noise and signal detection in climatic time series. Clim. Change 33, 409–445.

Miknis, F.P., 1995. Methods of oil shale analysis. NATO ASI Ser., Ser. C 455, 191–209.

Muller, R.A., MacDonald, G.J., 2000. Ice Ages and Astronomical Causes; Data, Spectral Analysis and Mechanisms. Praxis Publishing, Chichester, UK. 318 pp.

Olsen, P.E., Kent, D.V., 1999. Long-period Milankovitch cycles from the Late Triassic and Early Jurassic of eastern North America and their implications for the calibration of the early Mesozoic time-scale and the long-term behaviour of the planets. Philos. Trans. R. Soc. Lond. Ser. A 357, 1761–1786.

Oriel, S.S., Tracey Jr., J.I., 1970. Uppermost Cretaceous and Tertiary stratigraphy of Fossil Basin, southwestern Wyoming. U. S. Geol. Surv. Prof. Pap. 635, 53.

Paillard, D., Labeyrie, L., Yiou, P., 1996. Macintosh program performs time-series analysis. EOS Trans. AGU 77, 379. URL: http://www.agu.org/eos_elec/96097e.html.

Pälike, H., Laskar, J., Shackleton, N.J., 2004. Geologic constraints on the chaotic diffusion of the solar system. Geology 32, 929–932.

Pälike, H., Frazier, J., Zachos, J.C., 2006a. Extended orbitally forced palaeoclimatic records from the equatorial Atlantic Ceara Rise. Quat. Sci. Rev. 25, 3138–3149.

Pälike, H., Norris, R.D., Herrle, J.O., Wilson, P.A., Coxall, H.K., Lear, C.H., Shackleton, N.J., Tripati, A.K., Wade, B.S., 2006b. The heartbeat of the Oligocene climate system. Science 314, 1894–1898.

Pietras, J.T., Carroll, A.R., Singer, B.S., Smith, M.E., 2003. 10 k.y. depositional cyclicity in the early Eocene: stratigraphic and ^{40}Ar/^{39}Ar evidence from the lacustrine Green River Formation. Geology 31, 593–596.

Pietras, J.T., Carroll, A.R., 2006. High-resolution stratigraphy of an underfilled lake basin: Wilkins Peak Member, Eocene Green River Formation, Wyoming, U.S.A. J. Sediment. Res. 76, 1197–1214.

Preto, N., Hinnov, L.A., 2003. Unraveling the origin of carbonate platform cyclothems in the Upper Triassic Durrenstein Formation (Dolomites, Italy). J. Sediment. Res. 73, 774–789.

Prothero, D.R., 1996. Magnetic stratigraphy and biostratigraphy of the middle Eocene Uinta Formation, Uinta Basin, Utah. In: Prothero, D.R., Emry, R.J. (Eds.), The Terrestrial Eocene–Oligocene Transition in North America. Cambridge University Press, New York, United States, pp. 3–24.

Roehler, H.W., 1991a. Identification of oil shale and trona beds and their geophysical log responses in the Energy Research and Development Administration Blacks Fork No. 1 corehole, Eocene Green River Formation, southwest Wyoming. US Geol. Surv. Misc. Field Studies Map MF-2158, 1 sheet.

Roehler, H.W., 1991b. Correlation and depositional analysis of oil shale and associated rocks in the Eocene Green River Formation, greater Green River basin, southwest Wyoming. Misc. Invest. Ser.-U. S. Geol. Surv. I-2226 2 sheets.

Roehler, H.W., 1991c. Chart showing identification of oil shale and trona beds and their geophysical log responses in the Union Pacific Railroad Company El Paso corehole No. 44-3, Eocene Green River Formation, southwest Wyoming. US Geol. Surv. Misc. Field Studies Map MF-2188, 1 sheet.

Roehler, H.W., 1992a. Correlation, composition, areal distribution, and thickness of Eocene stratigraphic units, greater Green River basin, Wyoming, Utah, and Colorado. U. S. Geol. Surv. Prof. Pap. 1506-E, E1–E49.

Roehler, H.W., 1992b. Description and correlation of Eocene rocks in stratigraphic reference sections for the Green River and Washakie basins, southwest Wyoming. U. S. Geol. Surv. Prof. Pap. 1506-D, D1–D83.

Roehler, H.W., 1993. Eocene climates, depositional environments, and geography, greater Green River basin, Wyoming, Utah, and Colorado. U. S. Geol. Surv. Prof. Pap. 1506-F, F1–F74.

Sinks, D.J., Trudell, L.G., Dana, G.F., 1983. Oil shale sample locations and analyses, Southwest Wyoming and Northwest Colorado. Public Inf. Circ.-Geol. Surv. Wyo., vol. 22. Geological Survey of Wyoming, Laramie, Wyoming, United States. 26 pp.

Smith, M.E., Singer, B., Carroll, A.R., 2003. ^{40}Ar/^{39}Ar geochronlogy of the Eocene Green River Formation, Wyoming. Geol. Soc. Amer. Bull. 115, 549–565.

Smith, M.E., Singer, B.S., Carroll, A.R., Fournelle, J.H., 2006. High-resolution calibration of Eocene strata; ^{40}Ar/^{39}Ar geochronology of biotite in the Green River Formation. Geology 34, 393–396.

Smith, M.E., Carroll, A.R., Singer, B.S., 2008. Synoptic reconstruction of a major ancient lake system: Eocene Green River Formation, Western United States. Geol. Soc. Am. Bull. 120, 54–84.

Smoot, J.P., 1983. Depositional subenvironments in an arid closed basin; the Wilkins Peak Member of the Green River Formation (Eocene), Wyoming, USA. Sedimentology 30, 801–827.

Stanfield, K.E., Frost, I.C., 1949. Method of assaying oil shale by a modified Fischer retort. United States Bureau of Mines Report of investigations. U. S. Bur. Mines, 4477. 13 pp.

Sullivan, R., 1980. A stratigraphic evaluation of the Eocene rocks of southwestern Wyoming. Report of Investigations, Geological Survey of Wyoming, 20. Geological Survey of Wyoming, Laramie, WY, United States. 50 pp.

Torrence, C., Compo, G.P., 1998. A practical guide to wavelet analysis. Bull. Am. Meteorol. Soc. 79, 61–78.

Westerhold, T., Rohl, U., Laskar, J., Raffi, I., Bowles, J., Lourens, L.J., Zachos, J.C., 2007. On the duration of magnetochrons C24r and C25n and the timing of early Eocene global warming events: Implications from the Ocean Drilling Program Leg 208 Walvis Ridge depth transect. Paleoceanography 22, PA2201. doi:10.1029/2006PA001322.